Journal of Applied Physics

First-principles study of helium behavior in nickel with noble gas incorporation

Cite as: J. Appl. Phys. **127**, 175903 (2020); https://doi.org/10.1063/1.5145016
Submitted: 13 January 2020 . Accepted: 08 April 2020 . Published Online: 04 May 2020

Liang-Xiang Liao, Xun Zhang, Cui-Lan Ren, Zheng-De Zhang, He-Fei Huang, Guo-Hong Ma, and Ping Huai

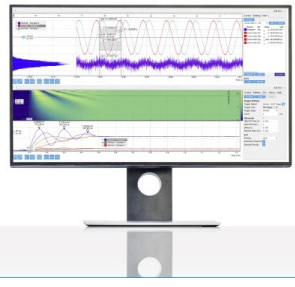

AIP Publishing

Journal of Applied Physics ARTICLE scitation.org/journal/jap

First-principles study of helium behavior in nickel with noble gas incorporation

Cite as: J. Appl. Phys. **127**, 175903 (2020); doi: 10.1063/1.5145016
Submitted: 13 January 2020 · Accepted: 8 April 2020 ·
Published Online: 4 May 2020

Liang-Xiang Liao,[1,2] Xun Zhang,[3] Cui-Lan Ren,[2,4,a)] Zheng-De Zhang,[2] He-Fei Huang,[2] Guo-Hong Ma,[1] and Ping Huai[2,3,5,a)]

AFFILIATIONS

[1]Department of Physics, Shanghai University, Shanghai 200444, China
[2]Shanghai Institute of Applied Physics, Chinese Academy of Sciences, Shanghai 201800, China
[3]School of Physical Science and Technology, ShanghaiTech University, Shanghai 201210, China
[4]Key Laboratory of Interfacial Physics and Technology, Chinese Academy of Sciences, Shanghai 201800, China
[5]Shanghai Synchrotron Radiation Facility, Shanghai Advanced Research Institute, Shanghai 201204, China

[a)]**Authors to whom correspondence should be addressed:** rencuilan@sinap.ac.cn. **Tel./Fax:** +86 21 33512449 and huaiping@sinap.ac.cn. **Tel./Fax:** +86 21 39194793.

ABSTRACT

The behavior of helium in nickel with noble gas atom (helium, neon, argon, krypton, and xenon) incorporations is systematically studied by using the first-principles method. The formation energies of noble gas atoms in nickel increase with atomic size increase from helium to xenon. All noble gas atoms considered in this work energetically prefer to stay at the substitutional sites when compared to the interstitial ones. The variations in formation energies among noble gas atoms can be mainly attributed to the steric effects caused by their incorporation. The chemical binding between nickel and noble gas atoms are further identified by their projected density of states. The substitutional noble gas shows a trapping effect on interstitial helium, and their binding energies also exhibit an approximately linear relation with their size. In addition, the effect of noble gas incorporation on helium clustering in nickel is studied. It shows that noble gas atoms attract small helium clusters and further repel the relatively larger ones. The results help to understand the influence of noble gas atoms on the fundamental helium behavior such as helium stability, trapping, and clustering in nickel and are also technologically important for further study on helium bubble nucleation under similar irradiation conditions.

I. INTRODUCTION

Nickel-based alloys have been widely accepted as candidates for structural materials in next generation nuclear systems such as molten salt reactors (MSRs).[1] They possess good high-temperature mechanical properties and excellent corrosion resistance properties to molten salts. However, nickel-based alloys are vulnerable to radiation-induced helium embrittlement or void swelling, which would reduce their mechanical properties and may further affect their service performance, and has become one of the main concerns in terms of safety and structural integrity.

By considering the source of helium in structural materials, it is known that helium can be produced directly from nickel or from ^{10}B impurity in nickel by transmutation reactions under neutron irradiations.[2] Helium ion irradiation is a commonly used approach to simulate the alpha decayed-helium produced by neutron in reactors. In addition, noble gas (NG) ion irradiations including Ar,[3–6] Kr,[7–9] and Xe[10–14] irradiations are also widely used to simulate the displacement cascades in materials under radiation. In recent years, multi-beam ion irradiation techniques such as helium co-implantation with heavy ion irradiation are utilized to simultaneously simulate the above-mentioned effects.[15,16] For ion irradiations with same beam energies, the projected range of He ion is much deeper when compared to that of Ar, Kr, and Xe, from the basic estimations predicted by Monte Carlo code SRIM.[17] Thus, proper beam energies should be used for multi-beam ion irradiation to ensure they have a overlapped irradiated region. Experimental investigations through accelerator-based ion irradiation techniques help to understand the irradiation-induced defect evolutions and long-term effect on the

macroscopic mechanical properties of materials.[5,11,14] However, the microstructural/defect evolutions at the atomic scale are still difficult to be well investigated up to now.

Fundamental studies on the stabilities and aggregation of helium and other noble gas including neon, argon, krypton, and xenon in metals at atomic scale are of great importance for the detailed understanding on the microscopic behavior of helium in nickel. The first-principles method based on the density functional theory (DFT), which can break through the limit of experiment, is an effective method to evaluate the structural or defect evolutions at the atomic scale. Many theoretical works have focused on the behavior of noble gas in alloys, especially on the behavior of helium. For example, Jiang *et al.*[18] systematically investigated the thermodynamical behavior of noble gas atoms in bcc transition metals including V, Nb, Ta, Cr, Mo, and W. It shows that the energetic behavior of noble gas atoms in the metals considered are dominated by the local relaxation processes rather than the chemical bindings between noble gas atom and metal matrix. Gai *et al.*[19] studied the formation of noble gas bubbles in bcc iron. The results showed that Ar and Xe prefer to occupy at the substitutional sites, and their diffusions in metal are via the vacancy-driven mechanism. With relatively higher migration energy barriers, Ar and Xe are relatively difficult to form bubbles when compared to the helium bubble. Nguyen-Manh *et al.*[20] studied the trapping effect of noble gas atoms on the helium clusters in bcc tungsten. Noble gas atoms prefer to stay at the tetrahedral site than the octahedral site, and their binding energies with the adjacent vacancy increase significantly from He to Xe. Kong *et al.*[21] reported the initial nucleation processes of interstitial He, Ne, and Ar clusters. It showed that the self-trapping process for Ne/Ar clusters are relatively easier to be triggered due to their stronger self-attractions when compared to that of helium clusters. The above-mentioned theoretical studies enrich the better understanding on the fundamental behavior of noble gas atoms in metals or alloys. However, the effect of noble gas on the helium stability and clustering in nickel-based alloy are still rarely explored until now.

In this work, the behavior of helium including its stability, binding, and clustering properties in nickel by consideration of noble gas (helium, neon, argon, krypton, and xenon) incorporation is investigated by using the first-principles method. The theoretical details are described in Sec. II. The main results about the helium stabilities and clustering are shown and discussed in Sec. III. The findings obtained at the atomic scale help a lot for the understanding of helium behavior in nickel and also technologically important to understand their macroscopic behavior such as helium bubble formation in nickel-based alloy under irradiation conditions.

II. THEORETICAL DETAILS

All calculations in this work were performed under the framework of the density functional theory as implemented in the Vienna *ab initio* simulation package (VASP).[22] The ion–electron interactions were treated by the projector-augmented wave (PAW) method.[23] The generalized gradient approximation (GGA) with the Perdew–Burke–Ernzerhof (PBE) method[24] is used to describe the exchange–correlation effects. The recommended standard potentials are used during the calculation, for which the valence electrons considered are listed as follows: Ni $3d^8 4s^2$, He $1s^2$, Ne $2s^2 2p^6$, Ar $3s^2 3p^6$, Kr $4s^2 4p^6$, and Xe $5s^2 5p^6$. An energy-cutoff of 400 eV is set for the plane wave expansion. Spin polarized calculations were performed during the simulations in consideration of the fact that nickel is magnetic.

A face-centered cubic (fcc) nickel lattice containing 108 atoms ($3 \times 3 \times 3$ supercells with simulation box size of $10.56 \times 10.56 \times 10.56$ Å) were used in the calculation. The Brillouin-zone integrations were performed using $5 \times 5 \times 5$ k-point mesh with the Monkhorst–Pack scheme.[25] The Methfessel–Paxton method with the smearing width of 0.2 was adopted throughout the structural optimization. The atomic positions were fully relaxed at constant volume until the force on each atom is less than 0.01 eV/Å. According to our convergence tests, such parameters for cutoff energy and k-point mesh are sufficient to give the converged results. For example, the differences of energy per atom for bulk nickel are less than 0.001 eV when compared to those using cutoff energies of 450 eV or higher. The differences of energy per atom for bulk nickel are also less than 0.001 eV between the present result and that of $7 \times 7 \times 7$ k-point mesh. The calculated lattice constant of nickel is 3.52 Å, which is well consistent with the previous experimental measurement of 3.524 Å[26] and calculated values of 3.516 and 3.523 Å, respectively.[27,28] Such parameters have also been proved to get a good convergence for the basic structural and physical properties of nickel. For example, the binding energy for nickel is calculated to be 4.84 eV, which is in good agreement with the previous theoretical calculation (4.84 eV)[29,30] and the experimental investigations (4.44 eV).[26] The vacancy formation energy is calculated to be 1.41 eV, which is also in good agreement with the previous result (1.37 eV).[29]

III. RESULTS AND DISCUSSION

A. The stability of noble gas atom in nickel

Initially, we investigate the stability of a noble gas in nickel. Three typically symmetrical occupation sites in fcc-nickel lattices were considered, the tetrahedral site (Tet), octahedral site (Oct), and substitutional site (Sub), as the schematic graph shown in Fig. 1(a). Here, the formation energies for the noble gas atoms at possible occupational sites are used to identify their stabilities in a metal matrix. The formation energy $E_{\text{int}}^{\text{f}}$ is expressed as the energy required for noble gas atom incorporation in interstitial sites,

$$E_{\text{int}}^{\text{f}} = E_{\text{NNi+NG}} - NE_{\text{Ni}} - E_{\text{NG}}, \tag{1}$$

where $E_{\text{NNi+NG}}$ denotes the energy of the supercell that contains N nickel atoms and a noble gas atom that locates at the interstitial site and E_{Ni} denotes the formation energy of bulk nickel. E_{NG} denotes the energy of an isolated NG atom that is calculated by placing it in a cubic cell with a side length of 15 Å. The formation energy $E_{\text{sub}}^{\text{f}}$ for a noble gas atom incorporation in the vacancy site, also being denoted as the substitutional site, is defined as

$$E_{\text{sub}}^{\text{f}} = E_{(\text{N}-1)\text{Ni+NG}} - (N-1)E_{\text{Ni}} - E_{\text{NG}}, \tag{2}$$

where $E_{(\text{N}-1)\text{Ni+NG}}$ is the energy of supercell with a noble gas atom incorporating in the substitutional site. A smaller value of formation energy means a more stable incorporation.

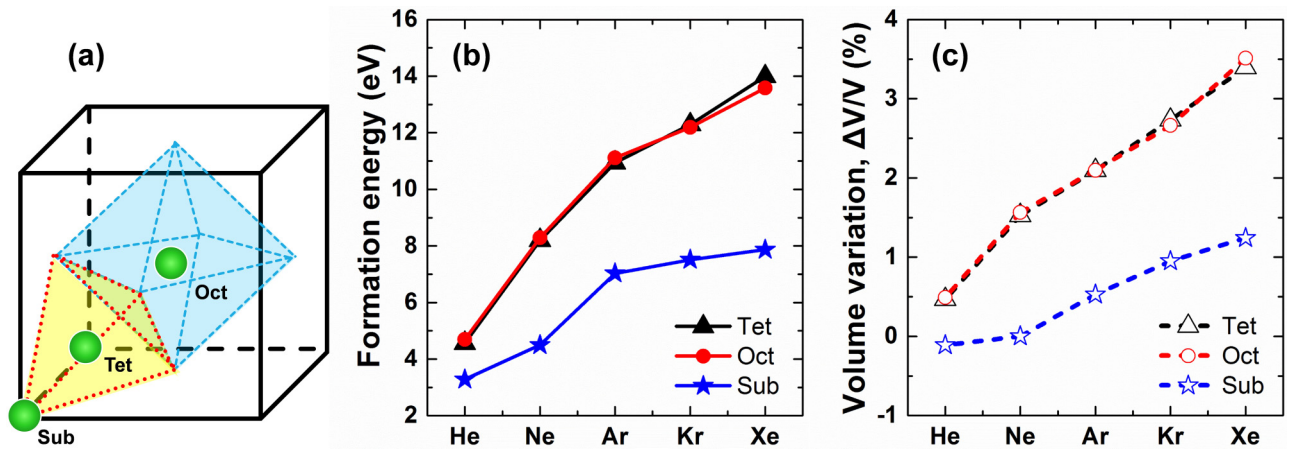

FIG. 1. (a) Schematic graph for the noble gas atoms (He/Ne/Ar/Kr/Xe) occupying at the Tet-, Oct-, and Sub-sites. The nickel atoms in fcc lattice sites are invisible for clarity. (b) The formation energies of a noble gas at various occupying sites. (c) The percentages of volume variation induced by a noble gas in nickel.

We first analyze the stability of helium atom in bulk nickel as a benchmark calculation. For the interstitial sites, it shows that helium is relatively stable when it occupies at the Tet-site with formation energy of 4.56 eV, approximately 0.14 eV lower than that at the Oct-site. Besides, with relatively lower formation energy of 3.27 eV, the Sub-site is the most energetically favorable site for helium in nickel, indicating that vacancy behaves as a sink for helium. These results are in good agreement with the previous DFT calculations.[29–31]

The formation energies of noble gas atoms at different occupying sites in nickel are shown in Fig. 1(b) and Table I. One can see that all noble gas atoms exhibit positive formation energies in all considered sites. Moreover, the formation energies increase quasi-linearly with their atomic size. Similar to helium, it is apparently shown that the formation energies for noble gas atoms at Tet- and Oct-sites are significantly larger than that at the substitutional site in bulk nickel, suggesting that the noble gas prefers to stay at the vacancy site. In another word, vacancy serves as a sink site for a noble gas atom. Taking xenon for example, the formation energy for xenon at Tet- and Oct-sites are calculated to be 13.98 and 13.57 eV, respectively, while it reduces to a relatively smaller value 7.86 eV at the vacancy site (Sub-sited Xe). The reduced formation energies for Sub-sited atoms can be attributed to that vacancy would help to release the local stress caused by the incorporation of a noble gas atom and the details will be shown later.

The above discussed formation energies are all calculated by using the fixed size and shape of the simulation box (see the Sec. II). However, when the noble gas atoms are introduced into bulk nickel, they would inevitably give rise to local stress and charge redistribution. Herein, we also considered the fully relaxed situation for a comparison, in which the volume variations are considered during the fully structural optimization. The formation energies calculated in the fully relaxed situations are also listed after the slash in Table I. One can note that the formation energies for the noble gas atoms at possible sites are all reduced more or less due to the full relaxation, and the reduction varies according to the types of noble gas as well as their occupying sites. For the interstitial noble gas atoms, the formation energy reductions for relatively smaller helium, neon, or argon are all approximately less than 3% when compared to the unrelaxed ones. For interstitial krypton and xenon, with the relatively larger atomic size, their formation energy reductions are about 5.3% and 6.9%, respectively. In contrast, when the noble gas atoms reside

TABLE I. The calculated formation energies (in eV) for noble gas atoms at different sites in bulk nickel under fixed box of the supercell or fully relaxation situation. The formation energies for helium are in comparison with the previous DFT calculations, as listed in parentheses.[29–31]

	Formation Energy (eV)				
Sites	He	Ne	Ar	Kr	Xe
Tet-site	4.56 (4.58,[a] 4.50,[b] 4.46[c])/4.52	8.19/7.94	10.94/10.62	12.29/11.64	13.98/13.01
Oct-site	4.70 (4.74,[a] 4.65,[b] 4.59[c])/4.66	8.29/8.11	11.11/10.78	12.19/11.56	13.57/12.78
Sub-site	3.27 (3.32,[a] 3.23,[b] 3.19[c])/3.28	4.50/4.49	7.02/6.95	7.51/7.45	7.86/7.69

[a]Torres *et al.*[29]
[b]Zu *et al.*[30]
[c]Hepburn *et al.*[31]

TABLE II. The percentages of volume variations induced by noble gas atom incorporation in typical occupying sites in bulk nickel. The corresponding volume variations are also listed in parentheses.

	Volume variation (%/ΔV)				
Sites	He	Ne	Ar	Kr	Xe
Tet-site	0.47% (5.49)	1.53% (17.96)	2.09% (24.66)	2.73% (32.14)	3.39% (39.91)
Oct-site	0.49% (5.78)	1.56% (18.41)	2.10% (24.67)	2.66% (31.32)	3.51% (41.34)
Sub-site	−0.11% (−1.31)	0% (0)	0.53% (6.21)	0.95% (11.17)	1.24% (14.61)

at a vacancy site, the energy reductions are less than 1% except for substitutional xenon, which is about 2.2% smaller than that of the unrelaxed situation.

Accordingly, the volume variation of noble gas atom incorporation in bulk nickel is defined as

$$\Delta V/V_0 = (V^{X}_{relax} - V_0)/V_0, \quad (3)$$

where V^{X}_{relax} and V_0 are the volumes of the supercell under full relaxation and fixed volume optimization, respectively. The values for the volume changes are listed in Fig. 1(c) and Table II. The fully relaxed supercell volume size increases with the size of noble gas increasing. It can be seen from Fig. 1(c) that the relative volume variations of Tet-, Oct-, and Sub-sited noble gas atoms increase monotonically with their atomic numbers, and the curve of volume variations possess similar trend with their corresponding formation energy curves. As also listed in Table II, the percentages of volume variations considered are less than 3.51%. For the interstitial noble gas atoms, the percentages of volume variations/expansions are 0.47%, 1.53%, 2.09%, 2.73%, and 3.39% for Tet-site, while they are 0.49%, 1.56%, 2.10%, 2.66%, and 3.51% for Oct-site, respectively. In the case that noble gas atoms occupy the substitutional sites, their volume shrink when compared with the original fixed volume for the smaller noble gas atom like helium, the volume remains unchanged for substitutional neon, and the volume slightly expands in a range of 0.53%–1.24% for Ar/Kr/Xe incorporation in substitutional sites. It shows that the mismatch in atomic size is one of the main concerns for the tendency of formation energies. The vacancy would help to release the local stress caused by noble gas incorporations and give rise to the relatively lower formation energies. Moreover, the mechanical effect caused by the existence of noble gas in nickel matrix would further affect the local NG–Ni interactions.

B. Projected density of states (PDOSs) analysis

Besides the above discussed mechanical effect caused by the mismatch of atomic size, the chemical interaction between helium and its surrounding host metal atom also plays an important role when it is incorporated in metal.[30] For a better understanding on the site preference of noble gas atoms and their interactions with the nickel matrix, the spin-resolved projected density of states (PDOSs) of a noble gas atom and its adjacent nickel atom for the occupied sites considered in this work are calculated and analyzed. The differential charge density analysis in previous theoretical studies indicated that there possesses polarized covalent bond components between metal and noble gas atoms, and the polarizations become significant from He to Xe.[18,30] It is also reported that the 3d state of transition metal dominates its chemical interaction between metal and helium.[30,32,33] Therefore, only the Ni 3d, NG s, and NG p states are plotted for clarity. The following discussion focus on the Ni 3d–He 1s and the Ni 3d–NG p (NG = Ne, Ar, Kr, and Xe) due to the electron distributions of NG atoms. The PDOS of Ni–He systems with Oct- and Tet-sited helium have been analyzed in our previous study.[32] Herein, we plot the PDOSs of the Ni–He system with Sub-sited helium for a comparison, as shown in Fig. 2(a). It shows that the Ni 3d states in systems with the existence of Oct-, Tet-, and Sub-sited helium possess similar behavior with each other. Compared to Oct- and Tet-sited helium, the broadened He s state for Sub-sited helium are shown in the range from −3.1 to −0.5 eV below the Fermi level. Such a greater overlapping area indicates their relatively stronger interaction with nickel atoms.

It is found that the PDOSs of Ni–He and Ni–Ne show similar behavior with each other, as well as the Ni–Kr and Ni–Xe systems. Thus, only the PDOSs for Ni–Ar and Ni–Xe systems are shown in Figs. 2(b) and 2(c) for clarity. Similar with the interaction between Ni–He, the larger overlapping area for Ni 3d–Ar 3p and Ni 3d–Xe 5p interactions for nickel with Sub-sited argon/xenon, indicating their relatively stronger interactions when compared to that of interstitial. From the formation energies of interstitial noble gas atoms shown in Fig. 1(b), it can be seen that Tet-sited He/Ne/Ar exhibit relatively lower formation energies when compared to that locating at Oct-sites, while the formation energies of Oct-sited krypton and xenon are slightly lower than that of Tet-sited ones. For Tet-sited Ar, resonance peaks of Ni 3p–Ar 3s states are in a range from −3.5 to −1.6 eV and those of Ni 3d–Ar 3p states are in a range from −3.0 to – 1.3 eV below Fermi level, as the black arrows pointed out. While the corresponding resonance peaks for Oct-sited argon exhibit as follows, the Ar 3s–Ni 3d interaction is shown in a range from −1.2 eV to Fermi level, and Ar 3p–Ni 3d states is shown in a range from −1.1 eV to Fermi level. The above analyses show that there are covalent bond components between argon and nickel, and the interaction for Tet-sited argon system is slightly stronger than that of Oct-sited one. While for the interstitial Xe–Ni systems similar hybrid states of Xe 5s–Ni 3p and Xe 5p–Ni 3p are shown [see Fig. 2(c)], small peaks for Oct-sited xenon located at −3.8 to −2.3 eV (Xe 5s–Ni 3p) and −3.5 to −2.3 eV (Xe 5p–Ni 3d) are found, which may suggest its relatively lower formation energy when compared to Tet-sited xenon.

Series of PDOS of Ni 3d states and NG p states for noble gas incorporation in Sub-, Tet-, and Oct-sites in nickel are shown in Figs. 2(d)–2(f), respectively. Apparently, the resonance areas of Ni 3d and NG p states indicate the components of covalent interactions between them. Besides helium, the main resonance peaks

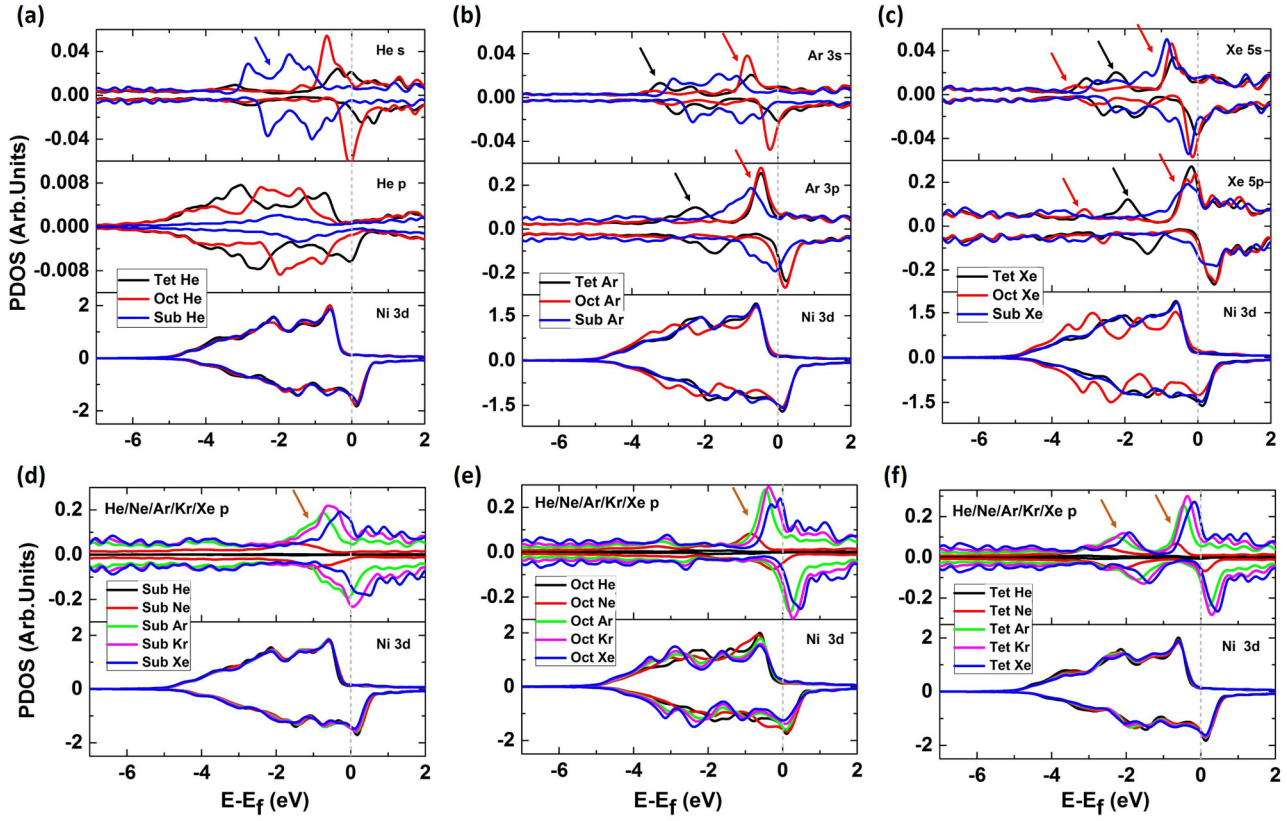

FIG. 2. PDOS of doped noble gas atom and its adjacent nickel atom in Ni–NG systems of Ni–He (a), Ni–Ar (b), and Ni–Xe (c) with three typical sites considered. The PDOS plots of NG P–Ni 3d state interactions for Ni–NG systems with NG atom doping at substitutional (d), octahedral (e), and tetrahedral (f) sites. The Fermi level is indicated by the dashed gray line at 0 eV. The positive direction of the *y* axis is taken from the upper spin orbit of the electron, and the negative *y* axis is the down spin orbit of the electron.

(or region), indicated by the arrows, show right shifts from Ne to Ar, Kr, and Xe, suggesting that the interaction between nickel and NG are gradually weakened from Ne to Xe, which are inconsistent with the results of formation energies aforementioned. The right shifts may arise from the gradually increased atomic size of NG atoms, which cause larger local stress in the nickel matrix. In addition, one can note that the Ni 3d states possess very similar behaviors in various systems with Sub- and Tet-sited noble gas atoms, while left shifts sequentially for nickel with Oct-sited noble gas are found [see Fig. 2(e)]. The NG–Ni bond lengths are approximately in a range of 1.9–2.3 Å for Oct-sited Ni–NG systems. Thus, slight variations in bond lengths would significantly affect their chemical interactions, in which the metallic bonds of nickel are weakened from He to Xe in nickel with Oct-sited NG atoms. In contrast, the Ni 3d states for Tet-sited NG–Ni systems exhibit similarity in the distances between NG atoms with their adjacent nickel atom (approximately 2.9–3.0 Å). From above analysis, one can see that the stabilities of noble gas atoms in nickel matrix are mainly dominated by the mechanical effects. The chemical interactions can be well understood from the covalent components between nickel and NG atoms.

C. Interaction between helium and noble gas impurity

In this section, we investigate the interaction between helium and noble gas in bulk nickel to further explore the trapping effects of noble gas on interstitial helium. As mentioned in Subsection III A, noble gas atoms all energetically prefer to stay at substitutional sites with relatively lower formation energies. Therefore, the noble gas atoms are considered to be placed at the vacancy site in nickel, forming He–V, Ne–V, Ar–V, Kr–V, and Xe–V pairs, respectively, as schematically shown in Fig. 3(a). While helium is inserted into the adjacent interstitial (Tet or Oct) positions by considering its smaller atomic size, the binding energies between interstitial helium and substitutional noble gas atoms are then written as

$$E^{b}_{NG-He} = E_{NNi+He} + E_{(N-1)Ni+NG} - E_{(N-1)Ni+NG+He} - E_{NNi}, \quad (4)$$

where E_{NNi+He} refers to the energy of the supercell with one helium atom occupying at the interstitial site. $E_{(N-1)Ni+NG+He}$ and $E_{(N-1)Ni+NG}$ denote the energies of supercells that contain one substitutional noble gas atom and with or without interstitial helium atom,

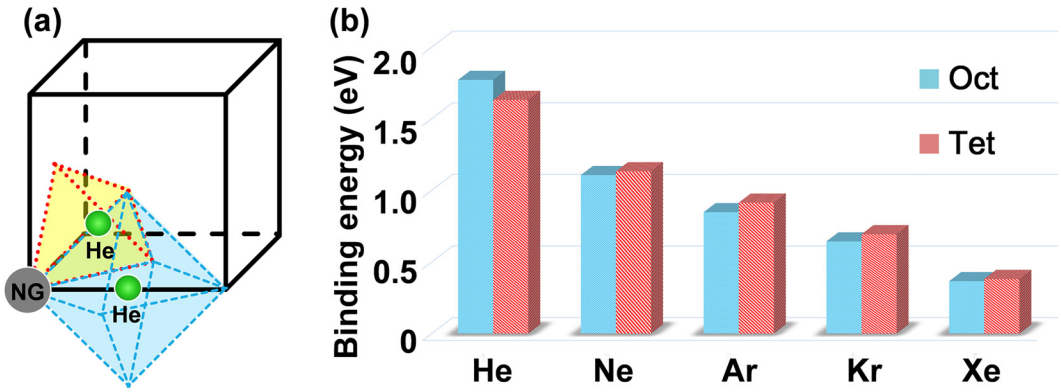

FIG. 3. (a) Schematic diagram for He–NG interaction systems, in which the noble gas atoms occupy at the substitutional site and helium at the interstitial site in the nickel matrix. The gray and green balls represent the noble gas and helium atoms, respectively. (b) The binding energies between substitutional noble gas atoms and adjacent interstitial helium.

respectively. According to such definition, the binding energy of the helium atom in the defect-free nickel supercell is calculated to be zero, and a positive binding energy indicates that helium atom and the doped noble gas atom are attractive to each other.

As shown in Fig. 3(b), the binding energies between Tet/Oct-sited helium and substitutional noble gas atoms exhibit a quasi-linear relation and go smaller for the relatively bigger noble gas atoms. Similar to the calculations by Nguyen-Manh *et al.* on the binding energy of interstitial helium and substitutional noble gas atoms in tungsten,[20] the results show that the binding energies of noble gas atoms and helium decrease with the increase in atomic size. For example, the binding energy between octahedral helium and substitutional helium is calculated to be 1.77 eV, and the value decreases to approximately 0.36 eV for the system contains octahedral helium and substitutional xenon, indicating that the attraction between substitutional noble gas atom and octahedral helium atom decreases sequentially in an order of helium, neon, argon, krypton, and xenon. Moreover, the binding energies between tetrahedral helium and substitutional noble gas atoms have similar tendency to that of octahedral helium. It is noticed that the binding energies of neon/argon/krypton/xenon and octahedral helium are slightly smaller when compared with that of tetrahedral helium atom. In contrast, by considering that noble gas atom is helium, it shows that the binding energy between tetrahedral helium and substitutional helium is slightly smaller than that of the octahedral helium. To explain this, we carefully checked the atomic configurations of the two systems. Substitutional helium is deviated from its initial position and formed helium–helium dimers at vacancy position. With He–He bond lengths are ~1.5 Å for both He_2 dimers along [111] and [100] directions, corresponding to the Tet- and Oct-sited helium atoms, respectively, slightly lower energy was found for the former one.

D. Trapping of helium clustering by noble gas impurity

The exploration of initial clustering and growth processes of helium bubbles at the atomic level is of critical importance to get fundamental understanding of interaction between small helium bubbles and metal matrix. It is known that vacancy can be easily formed under the non-equilibrium conditions like neutron/ion irradiation, and vacancy generally behaves as a sink for a helium atom or small helium clusters. In addition, the incorporation of foreign impurities like noble gases could also trap vacancy or helium from the introduced local lattice strain/distortion in matrix materials.[19,20,34] In this section, the effects of doped noble gas on helium clustering are clarified in detail. The models are designed as follows: noble gas atoms are placed at their most stable substitutional sites, while helium atoms are put into the first nearest neighbor (1NN) adjacent vacancy site one by one to identify their initial

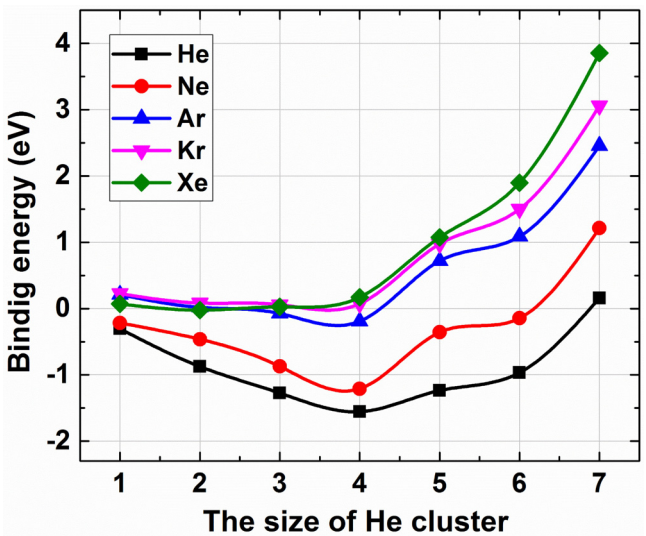

FIG. 4. Binding energies between helium clusters (He_nV with n up to 7) and their 1NN adjacent substitutional noble gas atom in nickel matrix.

nucleation processes. The helium clusters (expressed as He_nV) with $n < 8$ are considered to avoid the exaggerated stress caused by larger helium clusters. The calculated binding energies of helium clusters and noble gas atoms are defined as

$$E^{b}_{NG-nHe} = E_{(N-2)Ni+NG+nHe} - E_{(N-2)Ni+NG} - E_{(N-1)Ni+nHe} + E_{(N-1)Ni}, \quad (5)$$

where $E_{(N-2)Ni+NG+nHe}$ and $E_{(N-2)Ni+NG}$ are the energies of the supercell that contains a substitutional noble gas atom and with or without He_n clusters, $E_{(N-1)Ni+nHe}$ refers to the energy of the supercell that contains a vacancy and He_n cluster locating at vacancy site, and $E_{(N-1)Ni}$ is the energy of supercell containing monovacancy. The physical meaning of binding energy represents the trapping ability of the NG atom to helium clusters, and a negative value indicates their attractive interaction.

For each helium cluster, we investigated a series of possible atomic configurations and the most energetically stable structures are considered to identify their stabilities. The plots of binding energies of helium clusters in nickel with the presence of various noble gas atoms are shown in Fig. 4. It can be seen that for each substitutional noble gas, the binding energies go down first and then continue to increase with the helium clusters growing up. The minimum points of binding energy for helium, neon, and argon-doped models are found to be −1.56, −1.21, and −0.19 eV when the size of helium cluster reaches He_4, whereas binding energies around zero are found for He_nV–NG (Kr, Xe), and the minimum values of 0.06 eV (Kr) and −0.02 eV (Xe) are found for He_3 and He_2, respectively. The above binding energy analysis shows that there is a stronger clustering tendency for small helium clusters, and it gradually becomes energetically unfavorable and even repulsive when the helium cluster continue growth. For substitutional helium and neon, positive binding energies are found with $n > 6$ for helium clusters, indicating that the continue growth of helium clusters with $n \geq 7$ is energetically unstable. Moreover, a critical size of helium clusters of $n \geq 5$ for argon and krypton, while $n \geq 3$ for xenon, is also examined through their binding energies. The substitutional noble gas atoms energetically repel the helium clusters that is larger than their critical size. Such a phenomenon has also been found in other metals, such as the carbon/nitrogen/oxygen-doped nickel,[32] the interface area in tungsten,[35] the vacancy site in tungsten,[36] and so on.

One can also see that steric effects are found in Ni–NG–helium systems from the above analysis. On the one hand, the substitutional helium exhibits the strongest attraction to He_nV clusters followed by neon, argon, krypton, and xenon; on the other hand, the critical helium cluster size gradually decreases for the substitutional noble gas atoms from helium to xenon. When a noble gas atom is incorporated into a vacancy site, its 1NN adjacent vacancy could hold a limited number of helium atoms with a self-trapping process. The doped noble gas atoms will eventually repel the helium clusters with helium clusters growing up. It can also be speculated that helium clusters in vacancies may mutate more vacancies with the continued growth of helium clusters, in which the significant lattice distortions inevitably give rise to the deviation of nearby nickel atoms from their lattice position and further emit self-interstitial atoms.[21]

IV. CONCLUSIONS

First-principles calculations have been carried out to investigate the behavior of helium including its stabilities, binding, and clustering in nickel with the incorporation of noble gas atoms such as helium, neon, argon, krypton, and xenon. It shows that the formation energies of noble gas atoms at various incorporation sites in nickel increase from helium to xenon with an approximately linear relationship. Compared with the interstitial sites, the substitutional sites are the most energetically favorable sites for all noble gases considered. The variations in formation energies among different noble gas atoms can be mainly attributed to the steric effects originated from lattice distortion caused by the incorporation of noble gas atoms. The projected density of states for various Ni–NG systems are also analyzed to identify their chemical binding. The binding energies between substitutional site noble gas atoms and interstitial helium decrease with the increase of atomic sizes. Besides, trapping effects for all noble gas atoms on helium clusters are found, in which noble gas atoms attract small helium clusters and repel larger ones. For substitutional helium and neon, positive binding energies with He_nV clusters for $n > 6$ are found, while for argon, krypton, and xenon, positive binding energies with He_nV clusters appear when $n > 4$. The above results not only provide preliminary explanations for the difference behavior of noble gas in nickel, they also give an improved understanding on the behavior of helium bubble nucleation in nickel under similar irradiation conditions.

ACKNOWLEDGMENTS

This work was partially supported by the strategically Leading Program of the Chinese Academy of Sciences under Grant No. XDA02040100 and by the National Natural Science Foundation of China under Grant Nos. 11805256 and 11975304. The authors acknowledge the TMSR Supercomputer Center and ShanghaiTech University High Performance Computing Public Service Platform for providing computing resources. The authors thank Dr. Chang-Ying Wang from Changzhou Institute of Technology, China, for helpful discussion.

REFERENCES

[1]K. L. Murty and I. Charit, J. Nucl. Mater. **383**, 189 (2008).
[2]Y. Dai, G. R. Odette, and T. Yamamoto, in *Comprehensive Nuclear Materials* (Elsevier, 2012), pp. 141–193.
[3]P. Liu, Q. Zhan, W. Hu, Y. Jia, W. Han, X. Yi, and F. Wan, Nucl. Mater. Energy **13**, 99 (2017).
[4]G. Choudhuri, P. Mishra, S. Basu, N. Gayathri, P. Mukherjee, V. Kain, D. Mukherjee, D. Srivastava, and G. K. Dey, J. Nucl. Mater. **514**, 12 (2019).
[5]B. Su, H. Liang, G. Liu, Z. Huang, X. Liu, Z. Chen, and D. Y. W. Yu, J. Eur. Ceram. Soc. **38**, 2289 (2018).
[6]X. Huang and Y. Shen, J. Nucl. Mater. **461**, 1 (2015).
[7]Y. Miao, J. Harp, K. Mo, S. Bhattacharya, P. Baldo, and A. M. Yacout, J. Nucl. Mater. **484**, 168 (2017).
[8]J. C. Haley, S. A. Briggs, P. D. Edmondson, K. Sridharan, S. G. Roberts, S. Lozano-Perez, and K. G. Field, Acta Mater. **136**, 390 (2017).
[9]H. Jiang, Z. Duan, X. Zhao, B. Zhang, and P. Wang, Appl. Surf. Sci. **498**, 143821 (2019).
[10]J. Li, H. Huang, G. Lei, Q. Huang, R. Liu, D. Li, and L. Yan, J. Nucl. Mater. **454**, 173 (2014).

[11]S. J. Zhang, D. H. Li, H. C. Chen, G. H. Lei, H. F. Huang, W. Zhang, C. B. Wang, L. Yan, D. J. Fu, and M. Tang, J. Nucl. Mater. **489**, 180 (2017).
[12]C. Yan, R. Wang, X. Dai, Y. Wang, X. Wang, G. Bai, and Y. Zhang, J. Nucl. Mater. **473**, 256 (2016).
[13]H. Chen, Y. Hai, R. Liu, L. Jiang, X. Ye, J. Li, W. Xue, W. Wang, M. Tang, L. Yan, W. Yin, and X. Zhou, Nucl. Instrum. Methods Phys. Res. Sect. B **421**, 50 (2018).
[14]H. F. Huang, D. H. Li, J. J. Li, R. D. Liu, G. H. Lei, S. X. He, Q. Huang, and L. Yan, Mater. Trans. **55**, 1243 (2014).
[15]E. Getto, Z. Jiao, A. M. Monterrosa, K. Sun, and G. S. Was, J. Nucl. Mater. **465**, 116 (2015).
[16]E. Getto, Z. Jiao, A. M. Monterrosa, K. Sun, and G. S. Was, J. Nucl. Mater. **462**, 458 (2015).
[17]J. F. Ziegler, M. D. Ziegler, and J. P. Biersack, Nucl. Instrum. Methods Phys. Res. Sect. B **268**, 1818 (2010).
[18]C. Jiang, Y. Zhang, Y. Gao, and J. Gan, Phys. Chem. Chem. Phys. **20**, 17048 (2018).
[19]X. Gai, R. Smith, and S. D. Kenny, J. Nucl. Mater. **470**, 84 (2016).
[20]D. Nguyen-Manh and S. L. Dudarev, Nucl. Instrum. Methods Phys. Res. Sect. B **352**, 86 (2015).
[21]X.-S. Kong, Y. You, X. Li, X. Wu, C. S. Liu, J.-L. Chen, and G. N. Luo, Nucl. Fusion **56**, 106002 (2016).
[22]G. Kresse and J. Furthmuller, Phys. Rev. B **54**, 11169 (1996).
[23]P. E. Blöchl, O. Jepsen, and O. K. Andersen, Phys. Rev. B **49**, 16223 (1994).
[24]J. P. Perdew, K. Burke, and M. Ernzerhof, Phys. Rev. Lett. **77**, 3865 (1996).
[25]H. J. Monkhorst and J. D. Pack, Phys. Rev. B **13**, 5188 (1976).
[26]C. Kittel, *Introduction to Solid State Physics*, 8th ed. (Wiley, New York, 2005).
[27]E. H. Megchiche, S. Pérusin, J.-C. Barthelat, and C. Mijoule, Phys. Rev. B **74**, 064111 (2006).
[28]P. K. Nandi, M. C. Valsakumar, S. Chandra, H. K. Sahu, and C. S. Sundar, J. Phys. Condens. Matter. **22**, 345501 (2010).
[29]E. Torres, J. Pencer, and D. D. Radford, J. Nucl. Mater. **479**, 240 (2016).
[30]X. T. Zu, L. Yang, F. Gao, S. M. Peng, H. L. Heinisch, X. G. Long, and R. J. Kurtz, Phys. Rev. B **80**, 054104 (2009).
[31]D. J. Hepburn, D. Ferguson, S. Gardner, and G. J. Ackland, Phys. Rev. B **88**, 024115 (2013).
[32]X. Zhang, C.-L. Ren, H. Han, C.-B. Wang, H.-F. Huang, Y.-R. Yin, W. Zhang, G. Lumpkin, P. Huai, and Z.-Y. Zhu, J. Appl. Phys. **122**, 065901 (2017).
[33]X. Wu, X.-S. Kong, Y.-W. You, C. S. Liu, Q. F. Fang, J.-L. Chen, G.-N. Luo, and Z. Wang, Nucl. Fusion **53**, 073049 (2013).
[34]G.-Y. Huang, N. Juslin, and B. D. Wirth, Comput. Mater. Sci. **123**, 121 (2016).
[35]C. González and R. Iglesias, J. Nucl. Mater. **514**, 171 (2019).
[36]J. Boisse, A. De Backer, C. Domain, and C. S. Becquart, J. Mater. Res. **29**, 2374 (2014).